

Time-resolved x-ray diffraction study of laser-induced shock and acoustic waves in single crystalline silicon

K.-D. Liss,^{1,a)} T. d'Almeida,² M. Kaiser,^{3,4} R. Hock,⁵ A. Magerl,⁵ and J. F. Eloy⁶

¹The Bragg Institute, Australian Nuclear Science and Technology Organisation, Private Mail Bag 1, Menai, New South Wales 2234, Australia

²Department of Physics, Cavendish Laboratory, University of Cambridge, J. J. Thomson Avenue, Cambridge CB3 0HE, United Kingdom

³Swiss Light Source, Paul-Scherrer Institut, CH-5232 Villigen PSI, Switzerland

⁴Laboratoire de Spectroscopie Ultrarapide, Ecole Polytechnique Fédérale de Lausanne, ISIC, FSB-BSP, CH-1015 Lausanne, Switzerland

⁵Lehrstuhl für Kristallographie und Strukturphysik, Universität Erlangen-Nürnberg, D-91054 Erlangen, Germany

⁶European Synchrotron Radiation Facility, BP 220, F-38043 Grenoble Cedex, France

(Received 26 March 2009; accepted 21 July 2009; published online 31 August 2009)

A rod of single crystalline silicon has been subjected to high-power nanosecond laser pulses inducing ultrasonic and shock waves traveling into the bulk of the material. Stroboscopic time-resolved high-energy x-ray diffraction measurements were carried out *in situ* to probe for strain states in the bulk of the sample. First, a supersonic shock front is observed which moves faster than the longitudinal acoustic phonons. Following the shock front, a much slower bunch of waves travels along the crystal. The x-ray diffraction records obtained in different configurations reflect a strong dependence of the wave propagation on the sample geometry. These results offer an experimental approach for the investigation of coherent phonons, structural phase transformations, plastic deformations induced during shock peening, and for the development of x-ray free-electron-laser optics. © 2009 American Institute of Physics. [DOI: 10.1063/1.3204968]

I. INTRODUCTION

X-ray diffraction studies on crystalline solids under shock loading are motivated by the need to obtain direct insight into various structural and mechanical properties of solids at the microscopic level. Due to the significant technical improvements achieved within the past decade,¹ *in situ* quantitative laboratory diffraction measurements have become feasible at short time scales during shock loading. A significant number of experiments were carried out to address challenging issues involving transient mechanical effects in solids. In particular, real-time x-ray diffraction has proved useful for understanding elastic-plastic deformations,² anomalous mechanical response,³ and structural phase transitions.^{4,5}

On the other hand, mechanical processing, such as surface modifications through shot peening and laser peening mechanisms, are applied routinely to engineer the surface wear and fatigue properties of mechanical devices in aeroplanes.⁶ Fundamental and applied studies were performed in the past in order to investigate structural changes in metals and engineering materials by both projectile impact^{7,8} and laser pulse impact.^{9,10} Some dynamic results were then extracted by record of ultrasonic waves; however, most results were obtained *postmortem* by metallographic and diffraction studies of plastic deformation. Interestingly, plastic deformation in single crystal silicon induced by heat-assisted laser-shock peening was recently investigated¹¹ using *ex situ* techniques. However, little is known on the real-

time atomic displacements during the event of a shock wave. Generally, the ultrashort electromagnetic pulse generation and interaction with matter is a broad field across the research disciplines.¹²

The development of third generation synchrotron-based pump/probe techniques^{13,14} has permitted further progress, allowing time-resolved diffraction techniques to be used for various applications. Stroboscopic measurements were used to investigate sound fields^{15,16} and x-ray optical devices operating at the picosecond time scale.^{17,18} Similar stroboscopic techniques were applied to the study of phase transformations occurring over millisecond time scales, where the kinetics of the transformation is determined by the interactions between micrometer sized grains or domains.^{19,20} In particular, the use of high-energy x rays has allowed probing of bulk samples and collection of nanosecond x-ray diffraction data from laser-shock compressed solids, at different stages of the wave propagation, thus overcoming the limitations due to back surface measurements.^{21,22}

Within the context of the range of applications mentioned above, we have developed a synchrotron-based experimental setup for an *in situ* time-resolved study of laser-induced shock and ultrasound waves. Investigations of standing wave ultrasonic fields were previously carried out using this experimental configuration.^{15,16,23} In this article, we report time-resolved high-energy x-ray diffraction measurements within the bulk of a perfect single crystalline silicon target impacted by short laser pulses under different geometrical configurations.

^{a)}Electronic addresses: liss@kdliss.de and kdl@ansto.gov.au.

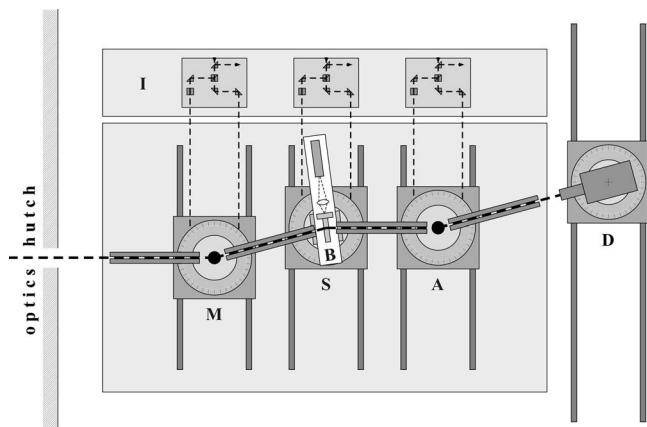


FIG. 1. General layout of the triple crystal diffractometer with monochromator (M), optional analyzer (A), detector (D), and interferometric angle encoders (I). The whole laser and sample system has been mounted onto an optical bench (B) on top of the sample stage (S).

II. EXPERIMENTAL METHOD

A. Experimental setup

The experiment was performed at the High Energy Beamline ID15A at the European Synchrotron Radiation Facility^{24,23} using the high-resolution triple axis diffractometer²⁵ of which a general setup is shown in Fig. 1. The white beam from the asymmetric-wiggler source was shaped and led to the monochromator (M), where a Bragg reflecting perfect Si crystal selects a wave vector k_i impinging onto the sample. Optionally, the diffracted wave vector k_f can be recorded by an open detector or through a Bragg reflection of an analyzer crystal, probing the beam distribution in a very narrow angular range. Operating with high order reflections in nondispersive mode and using a mechanically stable instrument allow probing for lattice strains down to 10^{-6} .^{25,23}

The sample was cut in one monolithic piece from a perfect silicon crystal with a rotational geometry along the [111] axis. It consists of a 5 mm thick plate of 30 mm diameter extended in a 45 mm long cylindrical rod of 2.75 mm diameter. The shape of the sample was designed to highlight the influence of its geometry on the compression process and on the timing of the wave propagation. As sketched in Fig. 2, the sample is mounted on the triple axis diffractometer with its [111] axis oriented along the laser beam impacting either from the plate or from the rod side. The incident laser pulses of 7 ns duration were delivered by a neodymium-doped yt-

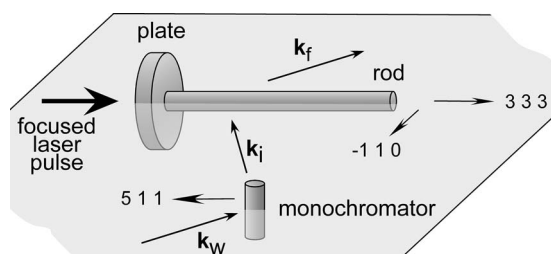


FIG. 2. Double crystal setup between monochromator and rod-plate shaped sample indicating the crystallographic directions and the x-ray and laser beams.

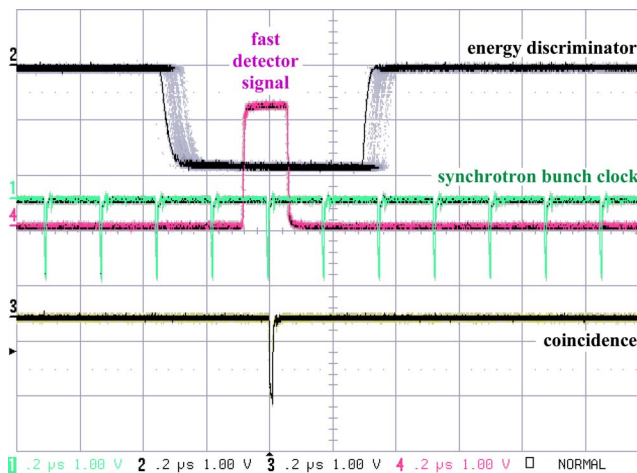


FIG. 3. (Color online) Coincidence of the different detector and synchrotron bunch clock pulses for the timing setup.

trium aluminum garnet solid state Q -switched laser of model Ultra / Big Sky Laser Technologies / Quantel at $\lambda = 1064$ nm with a peak irradiance of 100 GW/cm^2 and up to 25 Hz repetition rate. A lens focused the laser beam to about 0.5 mm diameter at the sample surface. The laser and optics were mounted on an extension arm which rotates and translates with the axis, ensuring that the laser impact on the sample surface remains unchanged throughout the measurements.

Stroboscopic timing was achieved by comparing the arrival time of a detected x-ray photon with the time of the previous laser shot and sorting the event into a corresponding time channel. The procedure is repeated as many times as needed to achieve sufficient statistics for each time channel.^{16,18} The output from a NaI scintillator equipped with a photomultiplier detector was split into a fast channel of <20 ns jitter and a slow channel for energy discrimination with 100 ns jitter. As shown in Fig. 3, triple coincidence with the bunch clock of the synchrotron allows to determine uniquely the time when the x-ray photon was created, giving a total jitter of 0.1 ns and leaving an unknown phase factor.

B. Measurements

A monochromatic x-ray beam of size $0.1 \times 0.1 \text{ mm}^2$ was used to collect data locally in Laue geometry integrating over the 2.75 mm diameter of the rod. Specific high-energy values of 113 and 169 keV were used to minimize the Bragg angles to 3.0° and 2.0° , respectively, and avoid spatial spreading in the Borrmann triangle. The specimen could be translated along the rod axis in order to probe for strain states at different distances from the impact surface.

We chose to monitor the Si 333 reflection with a scattering vector parallel to the sample axis because it matches ideally the Si 511 reflection of the monochromator. This ensures data collection in the nondispersive diffractometer mode with minimal perturbation from harmonics. A rocking curve of the sample at 169 keV is presented in Fig. 4. It exhibits a Lorentzian shape and a width of 0.40 arc. sec. in good agreement with the dynamical theory of diffraction. Time-resolved patterns were recorded 0.40 arc. sec. off each

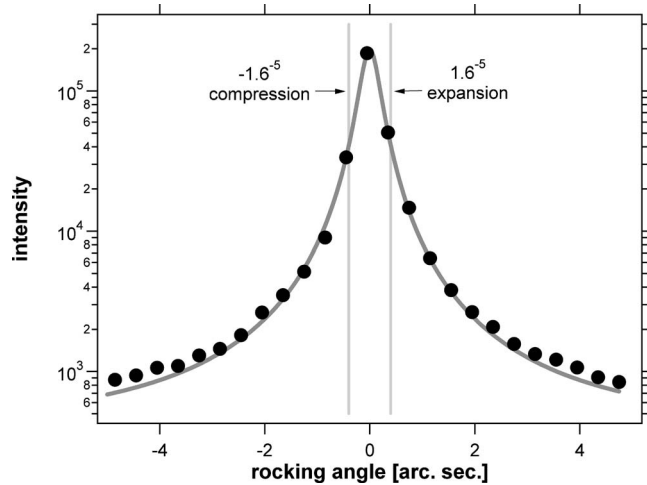


FIG. 4. Rocking curve of the Si 333 reflection of the sample against the monochromator showing an ideal Lorentzian shape and line width. The compressive and tensile strain positions where the time-resolved signals were collected are shown.

side of the peak corresponding to $\pm 1.6 \times 10^{-5}$ compressive or tensile strain. At times when these strain states are passed or included in a strain gradient, intensity increases in the time profile. Typical time patterns, here on the expansion side, are given in Figs. 5 and 6 for impact on the plate and on the rod, respectively. For impact on the plate, time patterns as a function of longitudinal position in the rod are shown on Figs. 7 and 8 for both lattice compression and expansion.

III. RESULTS AND DISCUSSION

Some general comments about the production of shock waves, and, in particular, laser-induced shock waves are needed prior to discussing the x-ray diffraction measurements performed in this work. Shock waves are generated as the result of a fast release of mechanical, chemical, nuclear, or radiative energy in relatively small regions. The actual shock wave results from the development of an initial large amplitude pressure wave traveling through a medium which

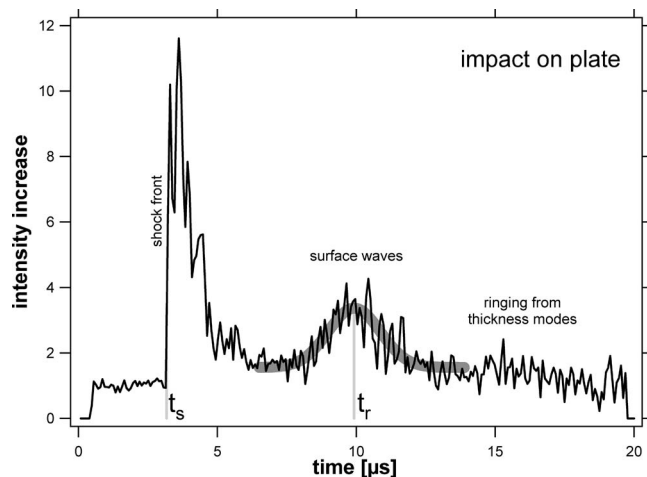


FIG. 5. Intensity normalized to unity for the undisturbed crystal as a function of time measured on the tensile strain side while impacted on the plate side. Arrivals of the shock front t_s and of the broad pulse distribution t_r are indicated.

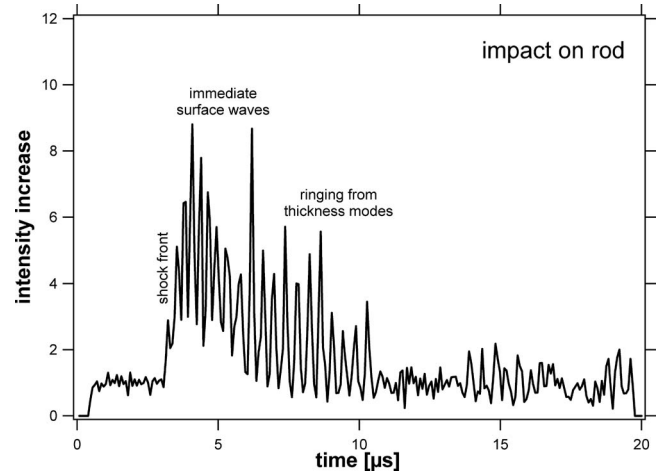


FIG. 6. Intensity normalized to unity for the undisturbed crystal as a function of time measured on the tensile strain side while impacted on the rod side. Ringing of the thickness modes is seen immediately after the arrival of the shock front.

becomes stiffer with compression. The process of laser-induced shock wave starts with the deposition and absorption of energy within a small region of the sample, near the impact surface. This region is subject to rapid heating, vapor-

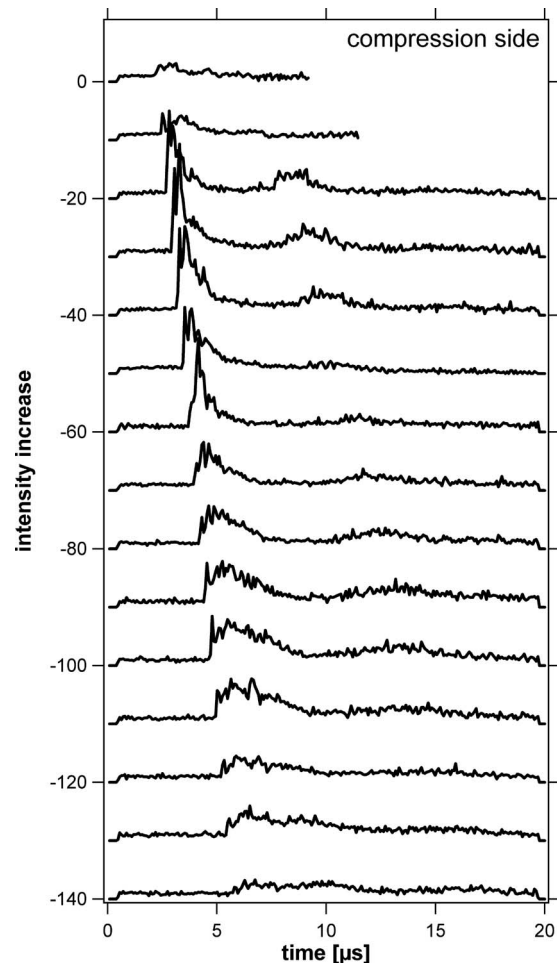


FIG. 7. Time dependent intensity profiles as in Fig. 5 as a function of position in the rod. The curves were recorded at intervals of 2.5 mm along the rod. The top curve is close to the impact surface.

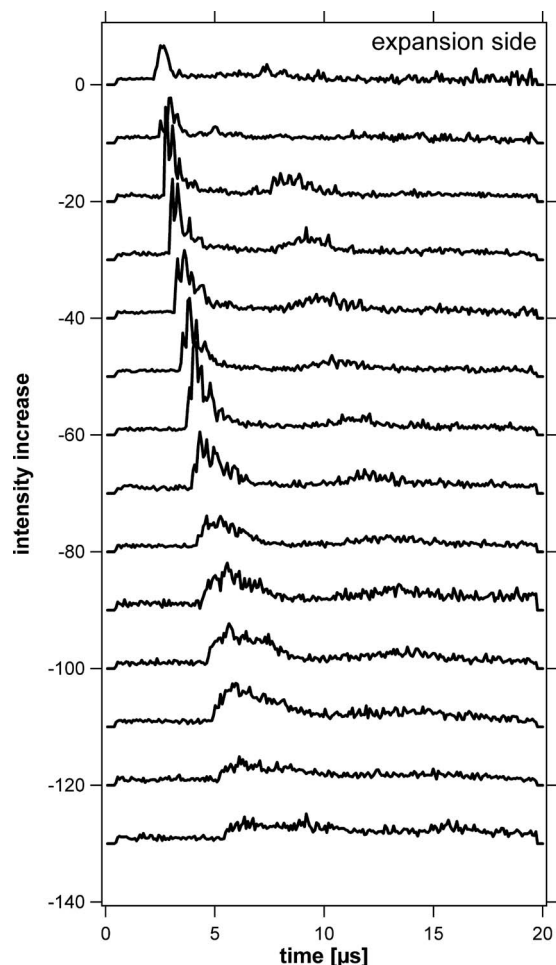


FIG. 8. Time dependent intensity profiles as in Fig. 6 as a function of position in the rod. The curves were recorded at intervals of 2.5 mm along the rod. The top curve is close to the impact surface.

ization, and ionization leading to the formation of plasma around the impact surface. Debris are expelled toward the plasma as they are ablated from the surface. In return, abrupt pressure is applied to the sample surface and shock waves are launched from the surface of the sample, as sketched in Fig. 9. The propagation of a shock wave is by nature a non-linear phenomenon. Laser-driven shock waves are often characterized by a wave profile which changes rapidly with propagation distance. Although the peak amplitude can be

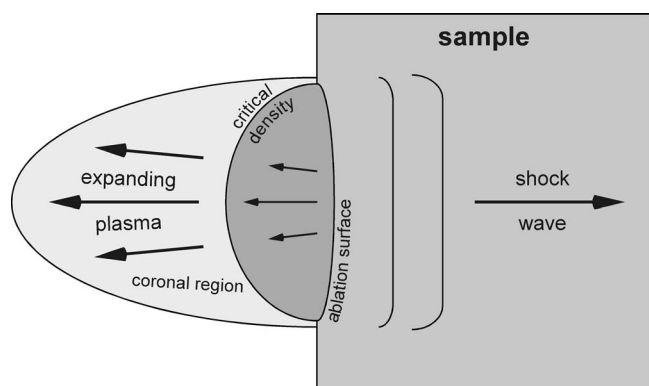


FIG. 9. Schematic view of shock wave generation as a result of laser impact.

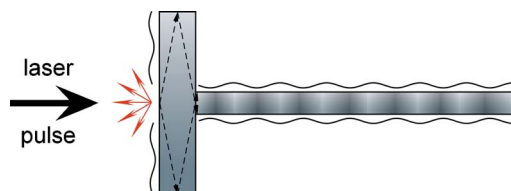


FIG. 10. (Color online) Suggested path for ultrasonic waves resulting from laser impact on the plate. Some longitudinal waves travel inside the plate along the dotted path and combine in a compressive way to produce thickness variations coupled to surface waves in the rod.

very high, the wave front is subject to rapid attenuation due to its narrow width, the top of the rarefaction fan behind the shock front traveling faster than the shock wave.²⁶

Figures 7 and 8 show the temporal profile of the diffracted intensity as a function of distance from the impact in the case of the laser beam impinging the plate side, on each side of the rocking curve. A selected pattern is given in Fig. 5. The record shows a sharp peak flank followed 7 μs later by a more or less pronounced “shoulder.” In Fig. 7, the flank corresponds to the arrival of the shock front, while in Fig. 8, it corresponds to the return of the release wave in the probed region. The shoulder is associated with the arrival of surface waves, slower by nature, but in the present case, also delayed because of the intentionally chosen sample geometry.

The attenuation of the shock front with increasing distance from impact results in the decay of the peak intensity. Had the x rays not been probing the bulk of the sample but conventionally the back surface, most of the information obtained at the early stages of the wave propagation would have been lost.

It appears from a more detailed examination of these intensity profiles, as shown in Fig. 5, that they exhibit superimposed oscillations with a periodicity of about 300 ns.

In contrast, impact on the rod side leads to a qualitatively different pattern, see Fig. 6. While the arrival of the shock front is still evidenced by an abrupt rise of intensity, surface modes follow immediately, superimposed by a ringing with roughly 300 ns period in the x-ray oscillations.

The differences observed between the two impact configurations can be explained as follows. Upon impact on the plate, both shock and surface modes are excited, as sketched in Fig. 10. Further longitudinal waves can travel into the plate and scatter back from the edge as indicated by the dotted path, recombining into radially compressive bulk modes coupled to surface waves in the rod. From the arrival times of both the shock and the surface waves as a function of distance from impact, compiled in Fig. 11, the wave velocities can be determined with a reasonable accuracy to the shock front velocity $c_s = 10066 \pm 54$ m/s and the ringing mode velocity coupled to the surface waves $c_r = 3390 \pm 97$ m/s. As expected, c_s is significantly higher than the longitudinal speed of sound of 9322 m/s in silicon along the [111] direction,^{27,28,16} which is one of the fingerprints of its nonlinear nature. While the shock wave travels through the bulk of the plate into and along the rod, the edge scattered wave has to follow the path in the plate and is therefore further delayed, in addition to its lower speed. The crystal being abruptly strained by the shock front results in a sharp

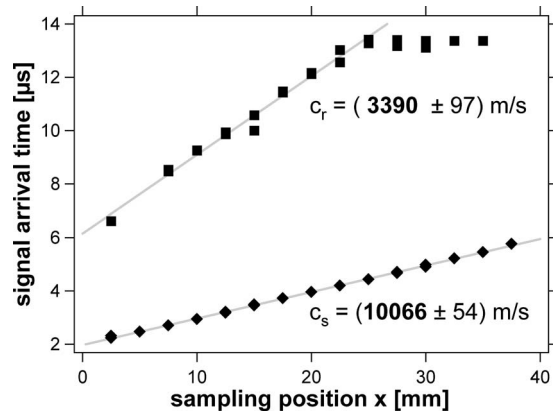


FIG. 11. Wave velocities c_s for the shock front and c_r for the wave bunch determined from the sampling positions and signal arriving times t_s and t_r from Figs. 5 and 7.

intensity rise at time t_s . Different modes and conversions are induced behind the shock front leading to the ringing and decay of the intensity peak. Several microseconds after the shock front, the scattered bulk waves traveled inside the plate and propagate along the rod, arriving in average around t_r in Fig. 7. As the sample is axial symmetric and the impact is produced on axis, the surface waves have a symmetric phase relationship when they travel along the rod. In particular, opposite surface regions across the diameter of the cylinder are elevated or depressed simultaneously which leads inevitably to tension or compression in the underlying bulk. In a simple model, a longitudinal standing bulk wave is established in the radial direction of the rod which is coupled to the axially traveling surface waves. As wave speeds in silicon are very anisotropic and only the in-scattering-plane components are accessed, full interpretation would exceed the purpose of this article. The complexity is further underlined by a dispersion and a beat which can be observed in Fig. 6. For a standing wave of large enough amplitude, the strain state cycles twice per ultrasound period through the strain state probed for by the x rays. Therefore, the ultrasound period must be twice as long as the observed x-ray ringing of 300 ns. Given the longitudinal sound speeds in silicon lying between 8433 and 9322 m/s (according to the crystalline direction), the ~ 2.75 mm diameter of the rod matches well the observed ultrasound period of 600 ns. For the case of impact on the rod, only minor delay of the surface waves is observed resulting in a quick increase in the ringing modes.

IV. CONCLUSION

The laser-induced elastic strain was examined in the bulk of a silicon target using time-resolved *in situ* high-energy x-ray diffraction. The passage of compressive and tensile waves at different locations was monitored within the sample through time-resolved x-ray diffraction measurements. Instabilities due to rarefaction were evidenced by the decay of the shock-induced mechanical effects with propagation distance. The supersonic shock wave velocity was determined from the diffraction data. A specific sample design has permitted to accentuate the delay of multiple scattered

waves generated by the laser impact and to highlight the influence of the sample geometry on the wave propagation. The measurements strongly suggest that when propagating along a cylindrical rod, surface waves are coupled to longitudinal bulk waves in the transverse direction.

The high-energy x-ray diffraction technique used in the present study offers the possibility to directly investigate a range of otherwise inaccessible shock-induced effects within the bulk of crystalline solids at the atomic level. Overcoming previous limitations due to back surface x-ray diffraction measurements should allow more detailed observations of transient mechanical and structural changes in materials subject to shock loading. It also lies the basis for the realization of x-ray optical switching devices²⁹ as they may be used to design Q-switching x-ray resonators and cavities.^{17,18} Such devices are valuable developing the equivalent of neutron Bragg reflecting cavities³⁰ for x-ray free-electron lasers. Last but not the least, these measurements illustrate the path for time-resolved *in situ* studies on the short and ultrashort time scales relevant to material engineering applications involving shock mechanisms, such as ball- and laser peening. As in the case of laser-induced surface acoustic wave studies, refinement of the ultrasound geometry with respect to phonon focusing and the tracking of linear and nonlinear physical parameters of materials shall be developed in the future.^{31,32}

ACKNOWLEDGMENTS

The authors would like to thank the company Quantel, Les Ulis, France for lending the laser solely for the purpose of the experiment.

- ¹Y. M. Gupta, K. A. Zimmerman, P. A. Rigg, E. B. Zaretsky, D. M. Savage, and P. M. Bellamy, *Rev. Sci. Instrum.* **70**, 4008 (1999).
- ²P. A. Rigg and Y. M. Gupta, *J. Appl. Phys.* **93**, 3291 (2003).
- ³A. Loveridge-Smith, A. Allen, J. Belak, T. Boehly, A. Hauer, B. Holian, D. Kalantar, G. Kyrala, R. W. Lee, P. Lomdahl, M. A. Meyers, D. Paisley, S. Pollaine, B. Remington, D. C. Swift, S. Weber, and J. S. Wark, *Phys. Rev. Lett.* **86**, 2349 (2001).
- ⁴T. d'Almeida and Y. M. Gupta, *Phys. Rev. Lett.* **85**, 330 (2000).
- ⁵S. J. Turneaure, Y. M. Gupta, and P. Rigg, *J. Appl. Phys.* **105**, 013544 (2009).
- ⁶W. Kaysser, *Surf. Eng.* **17**, 305 (2001).
- ⁷G. Naulin and J. P. Ansart, *J. Phys. Colloq.* **49**, C3-363 (1988).
- ⁸J. B. Hu, X. M. Zhou, H. Tan, J. B. Li, and C. D. Dai, *Appl. Phys. Lett.* **92**, 111905 (2008).
- ⁹R. Fabbro, P. Peyre, L. Berthe, and X. Scherpereel, *J. Laser Appl.* **10**, 265 (1998).
- ¹⁰K. Ding and L. Ye, *Surf. Eng.* **19**, 351 (2003).
- ¹¹G. J. Cheng, M. Cai, D. Pirzada, M. J. F. Guinel, and M. G. Norton, *ASME J. Manuf. Sci. Eng.* **130**, 011008 (2008).
- ¹²J.-F. Eloy, *Progress in Ultra-Short Electromagnetic Pulse Technology. A New Frontier in Physics* (Hermes-Penton Science, London/ Elsevier, New York/North-Holland, Amsterdam, 2002), pp. 1–253.
- ¹³S. Techert, F. Schotte, and M. Wulff, *Phys. Rev. Lett.* **86**, 2030 (2001).
- ¹⁴F. Schotte, S. Techert, P. Anfinrud, V. Srajer, K. Moffat, and M. Wulff, in *Third Generation Hard X-Ray Synchrotron Radiation Sources*, edited by D. Mills (Wiley, New York, 2002), pp. 345–401.
- ¹⁵K. D. Liss, A. Magerl, R. Hock, A. Remhof, and B. Waibel, *Europhys. Lett.* **40**, 369 (1997).
- ¹⁶K.-D. Liss, A. Magerl, R. Hock, B. Waibel, and A. Remhof, *Proc. SPIE* **3451**, 117 (1998).
- ¹⁷K.-D. Liss, R. Hock, M. Gomm, B. Waibel, A. Magerl, M. Krisch, and R. Tucoulou, *Nature (London)* **404**, 371 (2000).
- ¹⁸K.-D. Liss, R. Hock, M. Gomm, B. Waibel, A. Magerl, M. Krisch, and R. Tucoulou, *Proc. SPIE* **4143**, 78 (2001).
- ¹⁹G. Eckold, M. Hagen, and U. Steigenberger, *Phase Transitions* **67**, 219

- (1998).
- ²⁰K.-D. Liss, M. Kaiser, R. Currat, F. Denoyer, J. Hlinka, and R. Hock, *J. Phys. D: Appl. Phys.* **36**, A172 (2003).
- ²¹T. d'Almeida, M. Di Michiel, M. Kaiser, T. Buslaps, and A. Fanget, *J. Appl. Phys.* **92**, 1715 (2002).
- ²²K. Ichiyangi, S.-I. Adachi, S. Nozawa, Y. Hironaka, K. G. Nakamura, T. Sato, A. Tomita, and S.-Y. Koshihara, *Appl. Phys. Lett.* **91**, 231918 (2007).
- ²³K.-D. Liss, A. Bartels, A. Schreyer, and H. Clemens, *Textures Microstruct.* **35**, 219 (2003).
- ²⁴T. Tschentscher and P. Suortti, *J. Synchrotron Radiat.* **5**, 286 (1998).
- ²⁵K.-D. Liss, A. Royer, T. Tschentscher, P. Suortti, and A. P. Williams, *J. Synchrotron Radiat.* **5**, 82 (1998).
- ²⁶M. B. Boslough and J. R. Asay, in *High-Pressure Shock Compression of Solids*, edited by J. R. Asay and M. Shahinpoor (Springer, New York, 1993).
- ²⁷K. Y. Kim, W. Sachse, and A. G. Every, *J. Acoust. Soc. Am.* **93**, 1393 (1993).
- ²⁸A. G. Every, *Handbook of Elastic Properties of Solids, Liquids, and Gases* (Academic, New York, 2001), Vol. I, Chap. 1, pp. 3–36.
- ²⁹M. F. DeCamp, D. A. Reis, P. H. Bucksbaum, B. Adams, J. M. Caraher, R. Clarke, C. W. S. Conover, E. M. Dufresne, R. Merlin, V. Stoica, and J. K. Wahlstrand, *Nature (London)* **413**, 825 (2001).
- ³⁰M. Schuster, H. Rauch, E. Seidl, E. Jericha, and C. J. Carlile, *Phys. Lett. A* **144**, 297 (1990).
- ³¹V. V. Kozhushko and P. Hess, *Ultrasonics* **48**, 488 (2008).
- ³²P. Hess, *Diamond Relat. Mater.* **18**, 186 (2009).